Bone 150 (2021) 115995

Contents lists available at ScienceDirect

Bone

journal homepage: www.elsevier.com/locate/bone

Effects of anti-resorptive treatment on the material properties of individual canine trabeculae in cyclic tensile tests

Martin Frank [a,1], Andreas Grabos [a,b,1], Andreas G. Reisinger [c], David B. Burr [b], Dieter H. Pahr [a,c], Matthew R. Allen [b], Philipp J. Thurner [a,*]

[a] Institute of Lightweight Design and Structural Biomechanics, TU Wien, Gumpendorfer Straße 7, 1060 Vienna, Austria
[b] Department of Anatomy, Cell Biology & Physiology, Indiana University School of Medicine, 340 West 10th Street Fairbanks Hall, Suite 6200, Indianapolis, USA
[c] Department of Anatomy and Biomechanics, Division Biomechanics, Karl Landsteiner University of Health Sciences, Dr.-Karl-Dorrek-Straße 30, 3500 Krems an der Donau, Austria

ARTICLE INFO

Keywords:
Individual trabeculae
Anti-resorptive treatment
Material properties
Cyclic test
Microdamage

ABSTRACT

Osteoporosis is defined as a decrease of bone mass and strength, as well as an increase in fracture risk. It is conventionally treated with antiresorptive drugs, such as bisphosphonates (BPs) and selective estrogen receptor modulators (SERMs). Although both drug types successfully decrease the risk of bone fractures, their effect on bone mass and strength is different. For instance, BP treatment causes an increase of bone mass, stiffness and strength of whole bones, whereas SERM treatment causes only small (4%) increases of bone mass, but increased bone toughness. Such improved mechanical behavior of whole bones can be potentially related to the bone mass, bone structure or material changes. While bone mass and architecture have already been investigated previously, little is known about the mechanical behavior at the tissue/material level, especially of trabecular bone. As such, the goal of the work presented here was to fill this gap by performing cyclic tensile tests in a wet, close to physiologic environment of individual trabeculae retrieved from the vertebrae of beagle dogs treated with alendronate (a BP), raloxifene (a SERM) or without treatments. Identification of material properties was performed with a previously developed rheological model and of mechanical properties via fitting of envelope curves. Additionally, tissue mineral density (TMD) and microdamage formation were analyzed. Alendronate treatment resulted in a higher trabecular tissue stiffness and strength, associated with higher levels of TMD. In contrast, raloxifene treatment caused a higher trabecular toughness, pre-dominantly in the post-yield region. Microdamage formation during testing was not affected by either anti-resorptive treatment regimens. These findings highlight that the improved mechanical behavior of whole bones after anti-resorptive treatment is at least partly caused by improved material properties, with different mechanisms for alendronate and raloxifene. This study further shows the power of performing a mechanical characterization of trabecular bone at the level of individual trabeculae for better understanding of clinically relevant mechanical behavior of bone.

1. Introduction

Osteoporosis is defined as a reduction of bone mass and strength [1] and is conventionally treated with anti-resorptive drugs, such as bisphosphonates (BPs) or selective estrogen modulators (SERMs) [2]. These drugs reduce bone resorption [3], increase areal bone mineral density (aBMD) [4,5] and reduce the probability of osteoporotic fractures [6]. Although aBMD is commonly used as a surrogate parameter of treatment success, an increase of aBMD alone cannot solely account for fracture risk reduction. For instance, it has been determined that only 4% of the observed vertebral fracture risk reduction in raloxifene (a SERM) treatment was associated with an increase of aBMD [7]. Using animal models, the reduction of fracture risk has been linked to improved whole bone mechanics [8,9], like larger stiffness and strength, both for BP and SERM treatment [10–15], whereas only raloxifene treatment increased bone toughness [11,16]. As bone is hierarchically structured, its mechanical properties arise from the combination of bone architecture, mass and material properties [8]. The improved properties of BP-treated bone have been linked to an improved or at least

* Corresponding author.
E-mail addresses: frankm@ilsb.tuwien.ac.at (M. Frank), Andreas.Reisinger@kl.ac.at (A.G. Reisinger), dburr@iupui.edu (D.B. Burr), dieter.pahr@kl.ac.at (D.H. Pahr), matallen@iu.edu (M.R. Allen), philipp.thurner@tuwien.ac.at (P.J. Thurner).
[1] Authors contributed equally.

https://doi.org/10.1016/j.bone.2021.115995
Received 22 January 2021; Received in revised form 25 April 2021; Accepted 28 April 2021
Available online 1 May 2021

Abbreviations

ALN	Alendronate treatment group
CON	Control treatment group
RAL	Raloxifene treatment group
BP	Bisphosphonate
SERM	Selective Estrogen Receptor Modulator
aBMD	areal Bone Mineral density
E_∞	Long-term stiffness
E_{mx}	Maxwell stiffness
E_0	Instantaneous stiffness
p	Hardening exponent
R	Hardening stress
$\widehat{E}$	Apparent stiffness
$\widehat{\sigma}_{max}$	Maximum stress
$\widehat{\varepsilon}_{max}$	Strain at maximum stress
$\widehat{W}_{el}$	Elastic work
$\widehat{W}_{py}$	Post-yield work
TMD	Tissue mineral density
Tt.Ar.	Total area of trabeculae (microdamage staining)
D.A.	Damaged area of trabeculae (microdamage staining)
D.D.	Damage density (microdamage staining)

maintained trabecular architecture [17–19], accompanied by increased bone mass [10–12,14,20]. However, effects on the material properties have been less conclusively reported [8] and seem to be differently affected by BP and SERM treatments [21].

Thus, it is essential to perform a thorough characterization to detect potential changes in the material properties after BP and SERM treatment. These findings will enhance our knowledge about the rationale of the observed superior whole bone mechanics. So far, most studies have focused on the "elastic" behavior of cortical bone specimens using nanoindentation [22–24], bending [25–27] or bone microindentation testing [28]. Bone is a viscoelastic material [29–31] and especially characterization of physiological relevant loading scenarios, such as fatigue and impact [32], would be favorable. In particular, characterization of mechanical properties of trabecular bone tissue is needed, as osteoporotic fractures mostly occur in the vertebrae and the femoral neck [33], regions rich in trabecular bone. Previously, tensile tests of individual trabeculae were mainly performed on untreated specimens, and only one study tested samples after antiresorptive treatment [34].

The goal of the current study was to perform cyclic tensile tests of individual trabeculae close to fracture and to use a previously established rheological model [35] to determine elastic, viscous, yield, and ultimate properties, as well as the loss tangent together with ultimate strain and toughness of the tissue. Additionally, this test procedure allows the induction of microdamage in a defined experimental set-up in-situ, and, stopping experiments prior to sample failure further allows comparison of potential differences in microdamage accumulation of alendronate, raloxifene and control specimens. These procedures enable testing of the hypothesis that antiresorptive treatments influence the material properties and the damage behavior of trabecular bone.

2. Material and methods

2.1. Sample selection

Thoracic (T8-T12) vertebrae were obtained from non-ovariectomized skeletally mature female beagle dogs (average age at beginning of treatment: (1.3 ± 0.2) years) from a previous study [11]. These animals were treated orally for 12 months with clinically relevant doses of alendronate (ALN, 0.2 mg/kg/d), raloxifene (RAL, 0.5 mg/kg/d) or saline (CON, 1.0 mL/kg/d). All experiments were approved by the Indiana University School of Medicine Institutional Animal Care and Use Committee prior to initiating. Whole vertebrae were wrapped in tissue soaked with Hanks balanced salt solution (HBSS, pH = 7.4) and stored at −20 °C until testing. In total, 24 individual trabeculae were harvested from vertebrae of five CON animals, 28 trabeculae from vertebrae of five RAL-treated animals and 30 trabeculae from vertebrae of five ALN-treated animals.

2.2. Sample preparation and mechanical testing

Vertebrae were thawed at room temperature and soft tissue was removed with tweezers and scalpels. Samples were cut into 300 μm thick slices with a low speed saw (IsoMet, Buehler, Germany) and bone marrow was removed with a dental water jet (OralB, Germany). Selection, dissection and embedding of individual trabeculae were performed as described in detail previously [36,37]. All preparation steps were performed in HBSS (pH = 7.4) to keep samples hydrated. In brief, trabeculae were inspected with a stereo microscope (SZX10, Olympus Corporation, Japan) and selected for dissection if they appeared translucent and slender. However, in contrast to the previous studies [36,37] trabeculae in the present study were much shorter (~200 μm instead of 500 μm to 1000 μm) and appeared mostly plate-shaped, instead of rod-like. This might be attributed to different species (smaller animals have thinner trabeculae [74]), skeletal age and different anatomical locations (e.g. toe vs. vertebrae). Actual dissection was done with surgical scissors. After dissection, samples were imaged with micro-computed tomography (μCT) using a μCT100 (Scanco Medical AG, Switzerland) at a nominal resolution of 3.3 μm (integration time 200 ms, average data 3, voltage 55 kV, current intensity 145 μA and 1500 projections) to obtain trabecular geometry and tissue mineral density (TMD). For TMD determination the device was calibrated using five 6-mm-diameter hydroxyapatite cylinders of known density (0, 100, 200, 400, 800; whereby 800 is measured weekly as control to ensure actual validity). From segmented image data the trabecular geometry was determined as follows: the cross-sectional area at the thinnest location was measured, as trabeculae showed a curved, inhomogeneous shape. In a previous study [37], the effect of using the mid-slice (likely the thinnest location because of shaft curvature) and the average cross-sectional area (trabecular volume used for strain tracking divided by shaft length) on obtained stress was assessed. Here, stress based on the area at the mid-slice was overestimated with the same quantity as it was underestimated when based on the average area (compared to a linear elastic FE model). In the current study, the smallest cross-section was used to calculate stress (as done in Frank et al. [38]), in order to obtain the largest stress in the trabecular struts, which is likely the location were the struts will fail and further, were microdamage accumulation is concentrated (see Fig. 5). After μCT imaging, the end pieces of the samples were embedded in epoxy glue (see schematic inset in Fig. 1 – A, epoxy in yellow) using custom made silicone chambers. The resulting sample shape is compatible for mounting samples into the circular receptacles of the test set-up. For tensile testing, sample alignment is crucial, which was verified from two orthogonal planes. Before testing, samples were rehydrated for at least 2 h by putting them into HBSS. Then, samples were mounted in a previously established tensile test set-up [36,37] operated with a servo-electric load-frame (SELmini - 001, Thelkin AG, Switzerland), equipped with a 10 N load cell (HBM-S2M, Germany) with a relative error of 0.02% at full-scale output. This test set-up allowed testing of individual trabeculae in a wet, close to physiologic, environment, submerged in a water bath filled with HBSS. For sample alignment, a pre-load of 0.05 was applied, and it was verified by visual checking, if the gap between sample and sample holder was closed, and if a remaining pre-load was present after at least 10 s holding time (see supplementary material for more details and Fig. S1). Further, the alignment was also checked visually from the front view, before the actual test was started. Deviations in pre-load were caused by small

differences in the embedding but accounted for by linear extrapolation of stress-strain diagrams to the origin (see supplementary material and Fig. S3). Cyclic tensile loading was performed with an increasing step function (displacement rate of 0.01 mm/s, which corresponds to an average strain rate of 0.003 s^{-1} for the first loading cycle) as shown in Fig. 1 – A. Testing was stopped when the trabecula showed clear stress-whitening in its center (see Supplementary Fig. 2, Supplementary videos 1 and 2), as whitening has been associated with microdamage formation [39]. This way, microdamage could be induced and testing of samples stopped prior to failure.

2.3. Determination of mechanical tissue properties

Strain was determined from videography data obtained using a video camera (UI-3250CP-M-GL, IDS GmbH, Germany) in combination with a telescopic lens system (KITO-D zoom objective, mounted on a KITO-ADP-0.5 adapter, Kitotec GmbH, Germany). A digital image correlation algorithm was used to extract tensile strain of the trabecular strut [36,37] (see inset in Fig. 1 – A for a trabecular strut - the cylindrical, parallel part of individual trabeculae - with an applied speckle pattern). Determination of tissue material properties (instantaneous modulus (E_0), long-term modulus (E_∞), yield stress (σ_Y), hardening coefficient (p), hardening stress (R), ultimate stress (σ_u), viscosity (η) and loss tangent (tan(δ), at 1 Hz)) was done using a previously published rheological model and optimization algorithm [35]. In brief, the method is based on a 2-layer elasto-visco-plastic rheological model (see Fig. 1 – B) consisting of an elasto-plastic layer (Prandtl layer) and a visco-elastic layer (Maxwell layer). Hereby, the Prandtl layer is composed of an elastic spring with elastic modulus (E_{pr}) in series with a plastic slider, that starts deforming upon reaching the yield stress (σ_Y). The stress in this layer (σ_{pr}) increases exponentially (hardening coefficient (p)), until plateauing at the ultimate stress (σ_u, and can be calculated as: $\sigma_{pr} = \sigma_y + (\sigma_u - \sigma_y) \cdot (1 - e^{-p\varepsilon_p})$, where ε_p is the plastic strain ($\varepsilon > \varepsilon_Y$)). The Maxwell layer is built of an elastic spring with elastic modulus (E_{mx}) in series with a viscous damper with a coefficient of viscosity (η). If strain is applied in a quasi-static manner, stress in the Maxwell layer approaches zero and the model's stiffness is solely driven by the elastic spring in the Prandtl layer, which can be interpreted as the long-term modulus of the material (E_∞). In contrast, in instantaneous deformations, the model stiffness reaches $E_{pr} + E_{mx}$, which can be interpreted as the instantaneous modulus (E_0).

Further, apparent stiffness ($\widehat{E}$), yield strain ($\widehat{\varepsilon}_y$), apparent maximum stress ($\widehat{\sigma}_{max}$), apparent strain at maximum stress ($\widehat{\varepsilon}_{max}$), apparent elastic work ($\widehat{W}_{el}$) and apparent post yield work ($\widehat{W}_{py}$) where determined on the envelope curve to estimate material toughness and strength (see supplementary material, for more details). Hereby, yield strain ($\widehat{\varepsilon}_y$) is defined as the point of largest goodness of fit for a linear regression (R^2) in the linear region, as described in our previous tensile tests on individual trabeculae [36]. Hereby, the R^2 value is determined as a function of data window size; increasing the window in the linear region increases the R^2 value (lower residuals, see inset in Fig. S3), whereas increasing it in the non-linear region decreases the R^2 value (larger residuals). Elastic work is the area under the curve until $\widehat{\varepsilon}_y$, post yield work from $\widehat{\varepsilon}_y$ until the final point of the test.

It should be noted that evaluations done with the rheological model are based on engineering stress and strain, assuming geometric linearity. In contrast, evaluations done with the envelope curve are based on true stress and strain, as ultimate strains were in the range of 10%.

2.4. Microdamage labeling and evaluation

Microdamage labeling was done via en bloc staining with basic fuchsin, as described previously [40]. In brief, specimens were put into 70% ethanol (EtOH) for at least 48 h after mechanical testing. Then, samples were stained with basic fuchsin (J.T. Baker, USA) in a graded series of increasing EtOH concentrations (80%, 95%, and 100% EtOH) under 20-psi vacuum. The samples were stained for 2 h in each solution, where each solution was renewed after the first hour. Afterwards, samples were put twice into pure 100% EtOH for 30 min each under a 20-psi vacuum to remove residual fuchsin stain. Finally, samples were stored in 70% EtOH at room temperature. Stained samples were put onto glass microscopy slides and embedded in epoxy glue (UHU Endfest 300, UHU, Germany). As trabeculae were mounted on 2 mm thick epoxy circular end pieces (previously used for mechanical testing) the trabecular strut (see inset in Fig. 1A) was located about 1 mm below the surface, in the center. A hand-held miller (Dremel 400, Dremel, Germany) was used to remove excessive epoxy until the trabecular strut was almost visible, and verified under a stereo microscope (SZX10, Olympus Corporation, Japan). Next, samples were ground in two steps using sandpapers with grit numbers of 80 and 240 until the trabecula was reached. Then, sandpapers with grit numbers of 800, 1500 and 2400 were used each for 2 min to ensure an even, smooth surface for microscopy. Using this approach, the visible layer of the trabecular strut at the focal plane (after removal of parts of the strut) indicated an average strut diameter of (100 ± 37) µm, in comparison to a determined trabecular thickness of (101 ± 40) µm in µCT-measurements (before processing). As such, it was assumed that approximately half of the trabecular shaft was removed and that the central slice was investigated for microdamage analysis (a much lower diameter at the focal plane would indicate that only a small part of the strut would have been removed, see supplementary material and Fig. S5 fur further details). This verification was

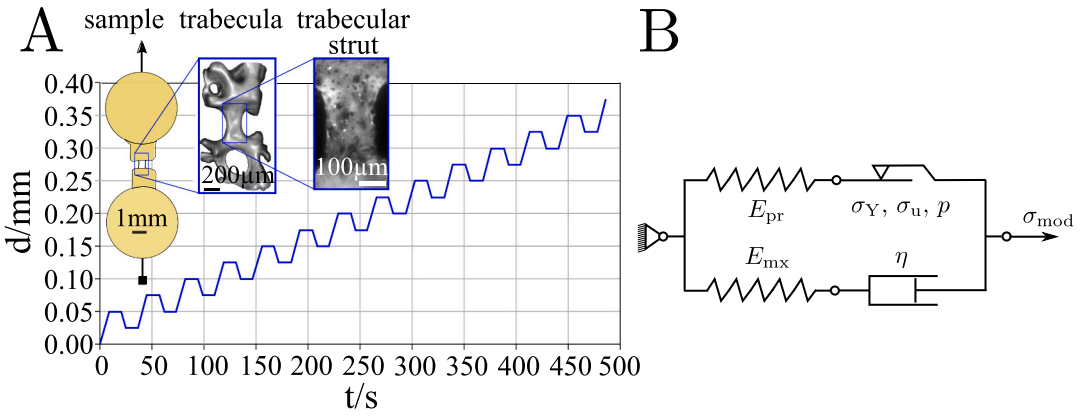

Fig. 1. A: Cyclic loading profile. The inset shows a schematic tensile test sample glued between circular end pieces (epoxy in yellow, individual trabecula magnified in the center – with residual bone - and trabecular strut with speckle pattern on the right). B: 2-layer elasto-visco-plastic rheological model ($E_{pr} = E_\infty$: Long-term stiffness, E_{mx}: Maxwell stiffness, σ_Y: Yield stress, σ_u: Ultimate stress, p: Hardening exponent, η: Viscosity, σ_{mod}: Model stress.). (For interpretation of the references to color in this figure legend, the reader is referred to the web version of this article.)

important, since microdamage was demonstrated to occur mainly in the center of trabecular struts [38,41], caused by an accumulation of advanced glycation end products [41].

Microdamage visualization was done with a confocal laser scanning microscope (CLSM, Zeiss Axiolab, Germany), operated by the Zeiss ZEN Black software for fluorescent materials. Due to the thickness of the trabeculae and the underlying epoxy (around 1 mm) only the surface was accessible for 2D microdamage analysis. Images were taken with a 20× epi-fluorescent objective (EC Plan-Neouar 20×/0.50 M27) at an excitation wavelength of 555 nm and using a rod-reflector (image pixel size: 1.25 μm). Image analysis was done with ImageJ (1.45 s, NIH, USA). The region of interest (ROI) was set to only contain the trabecular strut (corresponding to the boundaries of the strain tracking area). No linear cracks and only one cross-hatched area in one sample were visible and diffuse damage was predominantly present. Conventionally, microdamage has to be distinguished from lacunae and canaliculi, however, in the present microscopy slices, damage was so dense and intense that no lacunae or canaliculi could be identified in the central damaged areas (see Fig. 5). Thus, each image was segmented using the triangle threshold (auto) method in ImageJ. Then, the damage area (D.A.) was determined as the cumulative area of white pixels and the total area (Tt.Ar.) as all pixels within the trabecular ROI. Damage density (D.D.) was then computed as the ratio of D.A. to Tt.Ar.

2.5. Statistical analysis

Statistical analysis was done in SPSS (Version 26, IBM, USA). First, results were tested for normality with both, a Kolmogorov-Smirnov test combined with a Lilliefors Significance Correction and a Shapiro-Wilk test. As most data was not normally distributed, a non-parametric Independent-Samples Kruskal-Wallis Test (K.W.) was used to check for significant differences among the different groups and pairwise comparisons were made calculating asymptotic significance (2-sided tests) with a significance level of $\alpha = 0.05$. Significant values were adjusted by the Bonferroni correction for multiple tests. *p*-Values denoted with K.W. demonstrate the p-values obtained from the Independent-Samples Kruskal-Wallis Test.

Determination of the tissue material properties with the rheological model may result in non-physically meaningful values (due to the fact that it is an optimization approach). Thus, an outlier removal strategy, based on the interquartile range (IQR) test was performed on all three combined testing groups in two successive ways, as reported previously [35]. First, the IQR-test was applied to the root mean squared error (RMSE) of the fitting curve to remove overall bad computational fits. Second, the IQR-test was also applied to each obtained material property variable individually, to remove non-physically meaningful values.

3. Results

In total 71 tests were performed that showed a reliable deformation behavior during video recording (27 ALN, 22 CON, 22 RAL), with an average testing time of 164 s. However, this number also includes 7 (3 ALN, 4 CON) repeated experiments that were done with the same samples because of sample sliding in the initial test. Here, the stress-strain diagrams of the second trial were checked for a reliable behavior and obtained mechanical properties remained in a reasonable range, minimizing the risk that samples were pre-damaged in the first trial. Sequentially, only the second trials were included, and the first experiments were omitted. Visual inspection of obtained stress-strain diagrams resulted in a further elimination of 10 tests (5 ALN, 2 CON, 3 RAL), mainly because of issues in optical strain tracking. Sequentially, 54 out of 71 experiments (76.1%) were used for the envelope curve-based evaluation, to obtain the apparent mechanical properties. As the rheological model fitting should rely on similar experimental tests, only experiments that contained more than one loading and unloading cycle were included as model input. This resulted in further removal of 5 data sets (3 ALN, 2 RAL), leaving 49 stress-strain curves for model fitting. As such, overall bad model fittings were identified as outliers in the RMSE and were removed (8 in total), resulting in 41 remaining curves (57.7%) that were successfully evaluated with the rheological model (16 ALN, 13 CON, 12 RAL). Exemplary stress-strain diagrams of experiments and superimposed ones obtained with the rheological model are illustrated in Fig. 2, whereby selected curves were chosen to illustrate the main observed effects of the different treatment groups (as described in the following paragraph).

Alendronate treatment resulted in a significantly larger long-term (E_∞) and instantaneous stiffness (E_0), compared to control specimens (see Table 1 and Fig. 3). Although not significant, hardening stress (R, K.W. $p = 0.073$) and ultimate stress (σ_u, K.W. $p = 0.129$) tended to be larger as well. Similarly, the maximum apparent stress ($\widehat{\sigma}_{max}$) also showed a trend of being larger in the alendronate ($p = 0.103$) and raloxifene ($p = 0.079$) groups, compared to the control group. Strain at maximum stress ($\widehat{\varepsilon}_{max}$) and post yield work ($\widehat{W}_{py}$) were significantly larger in the raloxifene group compared to control ($p = 0.032$ and 0.002, respectively). Yield stress (σ_Y), apparent yield strain ($\widehat{\varepsilon}_Y$), apparent elastic work ($\widehat{W}_{el}$), Maxwell stiffness (E_{mx}), viscosity (η), hardening coefficient (p) and loss tangent ($\tan(\delta)$) were not statistically different among the subgroups.

Mean tissue mineral density (TMD) was significantly larger in the alendronate treatment group compared to raloxifene ($p = 0.010$), and showed a trend towards larger values in comparison to control ($p = 0.068$, see Fig. 4 – A and top of Table 2). TMD was significantly correlated with long-term stiffness (E_∞, $r_s = 0.59$, $p = 0.045$) for raloxifene-treated trabeculae, but not for control or alendronate-treated ones. In contrast, TMD was significantly correlated with Maxwell stiffness (E_{mx}, $r_s = 0.83$, $p = 0.001$) for alendronate-treated trabeculae, but not for control or raloxifene-treated ones (see Fig. 4 – B).

No significant differences were observed in the damage area (D.A.) or the damage density (D.D.) among the groups (see Fig. 5 – D and bottom part of Table 2). Selected basic fuchsin stained images for illustration of qualitatively similar microdamage accumulation are shown in Fig. 5 – A–C. Further, the number of cycles at damage detection, e.g. occurrence of whitening, was not significantly different among treatment groups ($p = 0.69$, 5 ± 3 cycles for ALN and RAL, 6 ± 4 cycles for CON).

4. Discussion

To the best of our knowledge, this is the first study that documents the effects of antiresorptive treatment on the tissue material properties of trabecular bone via testing of individual, hydrated trabeculae in tension. In summary, individual trabeculae showed a higher long-term modulus, instantaneous modulus and apparent modulus after one-year treatment with alendronate compared to control samples. In contrast, raloxifene treatment resulted in a significantly higher post-yield work and strain at maximum stress.

4.1. Alendronate treatment increases tissue modulus and strength

Apparent elastic modulus ($\widehat{E}$) was significantly larger ($p = 0.012$) in alendronate-treated samples, compared to control. This behavior is potentially related to a larger long-term stiffness (E_∞), Maxwell stiffness (E_{mx}) or viscosity (η). The rheological model discriminated among those effects, indicating that long-term stiffness (E_∞) was significantly larger ($p = 0.023$), whereas Maxwell stiffness (E_{mx}) remained non-significantly greater (K.W. $p = 0.171$). Instantaneous stiffness E_0 was also significantly larger ($p = 0.009$), while viscosity was not significantly affected. This finding is in agreement with the model predictions of Siegmund et al. [21] and an observed increase in indentation modulus of human trabecular iliac crest bone with increasing BP treatment duration [24]. On the contrary, the majority of previous studies found no significant

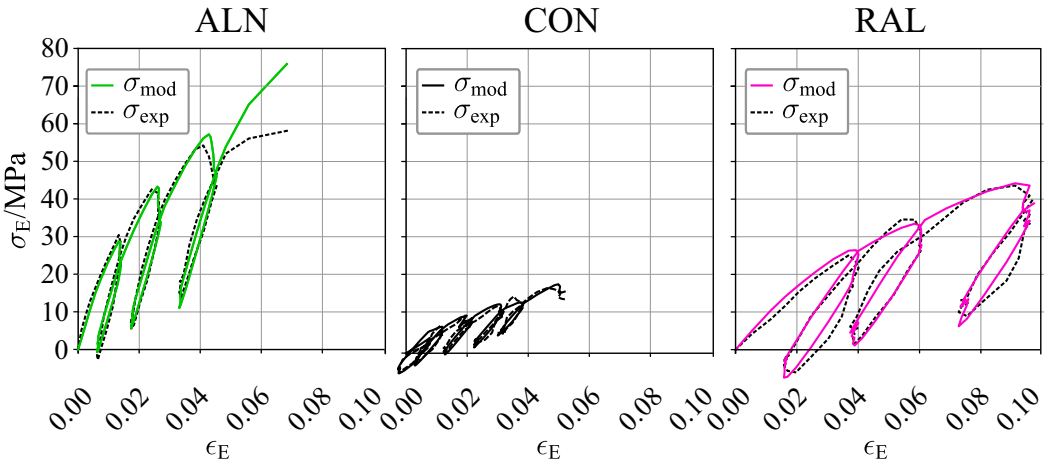

Fig. 2. Exemplary engineering stress-strain curves of alendronate (ALN), control (CON) and raloxifene (RAL) samples. σ_{mod} indicates the obtained stresses from the rheological model, σ_{exp} the calculated one from the experiment. Curves were selected to demonstrate the overall observed effects of the different treatments on the material proeprties and number of cycles at failure (here 4 for ALN and RAL, and 5 for CON).

Table 1
Determined mechanical tissue properties after alendronate (ALN) and raloxifene (RAL) treatment, compared to control (CON). E_∞: Long-term stiffness, E_{mx}: Maxwell stiffness, E_0: Instantaneous stiffness, σ_Y: Yield stress, p: Hardening coefficient, R: Hardening stress, σ_u: Ultimate stress, η: Viscosity, tan(δ): Loss tangent (at 1 Hz), $\widehat{E}$: Apparent stiffness, $\widehat{\varepsilon}_{max}$: Apparent strain at maximum stress, $\widehat{\sigma}_{max}$: Apparent maximum stress, $\widehat{W}_{el}$: Apparent elastic work, and $\widehat{W}_{py}$: Apparent post yield work. Mean values are indicated ±standard deviation. K.W. denotes the p-value obtained with the Kruskal-Wallis test. If K.W. shows a p-value < 0.05 then the actual p-values for group-wise comparisons are shown on the right (corrected for multiple testing). [a] illustrates a significant ($p < 0.05$) difference to CON.

Parameter	ALN	CON	RAL	K.W.	A-C	A-R	C-R
E_∞/GPa	1.8 ± 1.1[a]	0.8 ± 0.9	1.1 ± 1.2	0.018	0.023	0.137	1.000
E_{mx}/GPa	1.2 ± 0.7	0.7 ± 0.5	1.0 ± 0.8	0.171			
E_0/GPa	2.9 ± 1.3[a]	1.4 ± 1.2	2.1 ± 1.7	0.011	0.009	0.270	0.650
σ_Y/MPa	11 ± 5	10 ± 5	13 ± 8	0.627			
P	48 ± 51	128 ± 236	37 ± 56	0.781			
R/MPa	41 ± 28	35 ± 55	20 ± 15	0.073			
σ_u/MPa	55 ± 31	45 ± 53	32 ± 14	0.129			
η/GPas	6.6 ± 7.5	9.3 ± 11.2	6.1 ± 6.6	0.645			
tan(δ)	0.009 ± 0.005	0.008 ± 0.003	0.009 ± 0.003	0.467			
$\widehat{E}$/GPa	2.4 ± 1.2[a]	1.2 ± 0.8	1.6 ± 1.3	0.010	0.012	0.089	1.000
$\widehat{\varepsilon}_{max}$/%	7.7 ± 3.7	6.6 ± 4.2	10.3 ± 4.0[a]	0.032	1.000	0.246	0.032
$\widehat{\sigma}_{max}$/MPa	67 ± 28	48 ± 32	70 ± 30	0.049	0.103	1.000	0.079
$\widehat{W}_{el}$/(MJ/m^3)	0.07 ± 0.05	0.10 ± 0.09	0.07 ± 0.04	0.776			
$\widehat{W}_{py}$/(MJ/m^3)	2.9 ± 1.8	1.8 ± 1.8	4.4 ± 2.7[a]	0.003	0.171	0.411	0.002

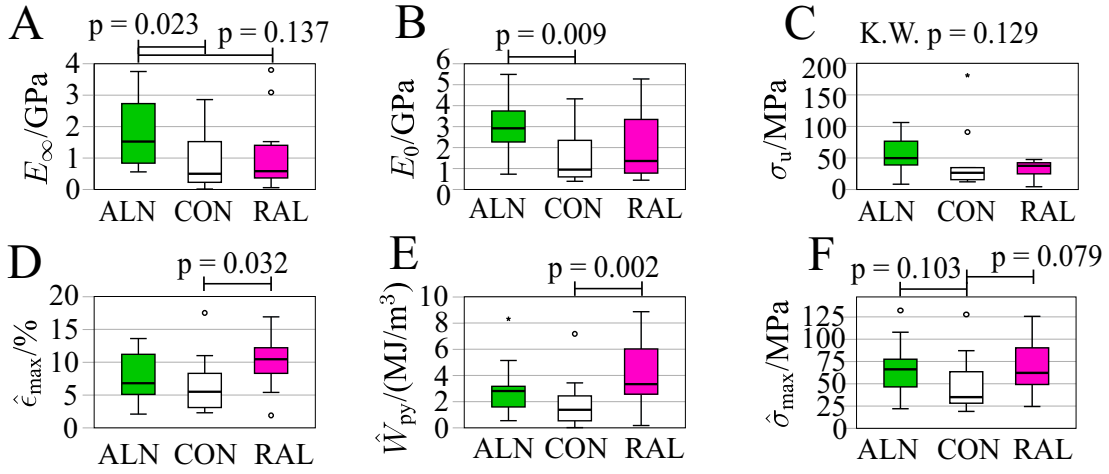

Fig. 3. Boxplots of material parameters after alendronate (ALN) and raloxifene (RAL) treatment, compared to control (CON) showing either statistically significant differences or trends close to significance. A: Long-term stiffness, B: Instantaneous stiffness, C: Ultimate stress, D: Apparent strain at maximum stress, E: Apparent post-yield work, F: Apparent maximum stress. Actual p-values are noted with bars.

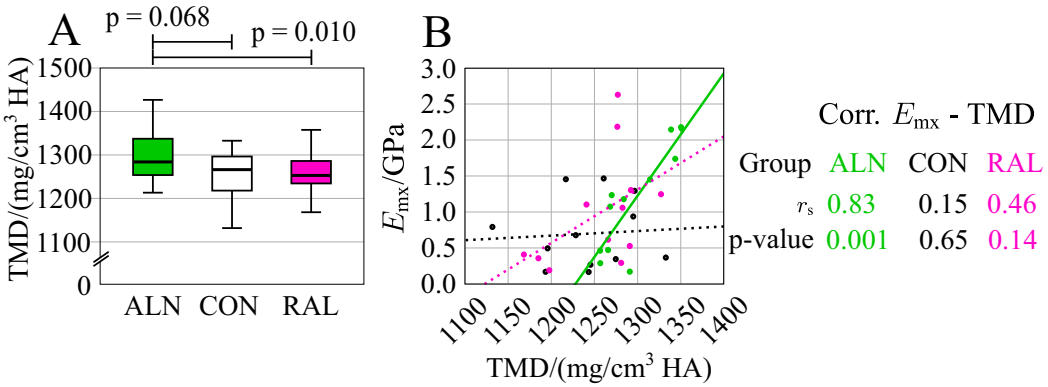

Fig. 4. A: Tissue mineral density (TMD) of alendronate (ALN), control (CON) and raloxifene (RAL) samples. B: Correlation of Maxwell stiffness (E_{mx}) with TMD, with noted spearman rank correlation coefficients and *p*-values on the right.

Table 2
Tissue mineral density (TMD), total area (Tt.Ar.), damage area (D.A.) and damage density (D.D.) of alendronate (ALN, A), control (CON, C) and raloxifene (RAL, R) samples. K.W. denotes the p-value obtained with the Kruskal-Wallis test. If K.W. shows a p-value < 0.05 then the actual p-values for group-wise comparisons are shown on the right (corrected for multiple testing). [b] illustrates a significant ($p < 0.05$) difference to RAl.

Parameter	ALN	CON	RAL	K.W.	A-C	A-R	C-R
TMD/(mg/cm^3 HA)	1294 ± 53[b]	1260 ± 47	1256 ± 4	0.008	0.068	0.010	1.000
Tt.Ar./μm^2	36,526 ± 12,874[b]	31,273 ± 10,601	26,863 ± 1,180	0.028	0.653	0.022	0.711
D.A./μm^2	11,368 ± 5,682	31,273 ± 10,601	9,190 ± 4,452	0.394			
D.D./%	32 ± 11	33 ± 12	35 ± 8	0.491			

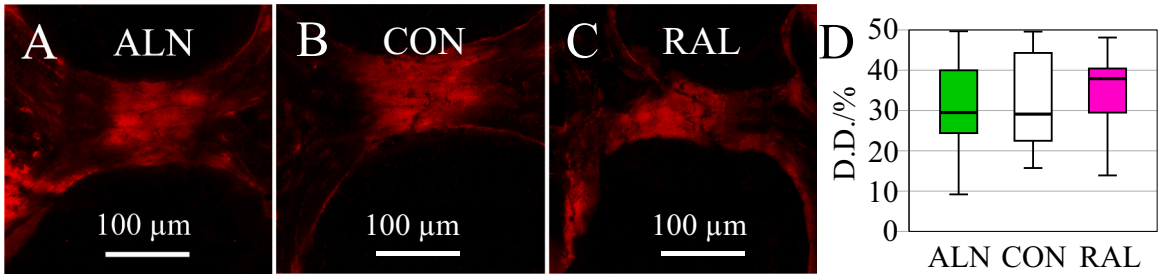

Fig. 5. Selected microscopy images of microdamage labeled samples with basic Fuchsin of alendronate (ALN, A), control (CON, B) and raloxifene (RAL, C) samples. D: Boxplots of damage density (D.D.).

change in tissue modulus after alendronate treatment, either in bending experiments on cortical bone from dogs [22,42], or humans [27], individual human trabeculae [34], or in nanoindentation experiments on cortical canine [22] or human bone [23]. In one study, indentation modulus was lower in cortical bone of iliac crest biopsies from alendronate-treated women diagnosed with osteoporosis compared to samples from osteoporotic untreated women [43], but in this study areas of matching TMD were comparatively assessed. Moreover, indentation and bending experiments cause undefined loading modes, consisting of a mixture of compression, tension and shear. Tensile experiments allow a more defined, homogeneous stress state, depending on the sample geometry and alignment.

Approaching the sub-mm length scale, Carretta et al. have shown that material properties of individual trabeculae from the same donor/animal and bone were significantly different between three-point bending and tensile tests [44]. Larger tissue stiffness (in terms of E_0, E_∞ and $\widehat{E}$) may be related to an increase in TMD [45,46], but also to an elevated amount of cross-linking in the collagen matrix [47,48]. However, it has to be stated that the collagen phase mainly affects the post-yield properties of bone [49–51] (and stiffness to a minor degree), whereas the pre-yield properties are mainly determined by the mineral phase, depending on the observed scale (more pronounced at the bulk scale, less at the tissue scale [52]). Tissue mineral density was almost significantly larger (K.W. $p = 0.068$) after alendronate treatment compared to control samples. As raloxifene treatment did not show any significant differences to control samples, RAL and CON groups were pooled for a further TMD evaluation. Here a significant difference ($p = 0.002$) between ALN and this pooled control group was detected, in accordance with previous studies of trabecular canine [10,11] and human [34,53] bone. Thus, it appears likely that the larger TMD is related to increased stiffness (E_0, E_∞ and $\widehat{E}$), as shown previously in trabecular porcine bone [54,55]. Surprisingly, there was no significant correlation between TMD and long-term (E_∞) or instantaneous stiffness (E_0), but only with Maxwell stiffness (E_{mx}, $r_s = 0.83$, $p = 0.001$). This rather high correlation of TMD and Maxwell stiffness could only be determined by the cyclic tensile tests, combined with the evaluation of the rheological model. Sequentially, according to the rheological model used, only the elastic part that is activated with increasing strain-rates is significantly correlated with tissue mineralization. It has to be mentioned that this correlation was very weak in the control group ($r_s = 0.15$, $p = 0.65$) and might be related to the large deviation of obtained values for E_{mx}, in combination with insignificant ($p = 0.171$) smaller values compared to the other groups.

A previous study using the same beagle dog model used in the cur-

rent study showed that alendronate treatment increased non-enzymatic cross-linking [56] in the canine vertebrae. Further, a higher amount of mature crosslinks was correlated to larger strength and stiffness in compression tests of human vertebral bone cores [48]. In the current study, stress at failure (σ_u) and maximum stress ($\hat{\sigma}_{max}$) showed insignificant trends to larger values (K.W. $p = 0.129$ and 0.103) after alendronate treatment. In contrast, previous studies from bending experiments on canine cortical [22,42,57] and human cortical bone [27], and human individual trabeculae [34], reported no significant change in tissue strength after alendronate treatment. Similarly, indentation hardness was either decreased (human cortical and cancellous [58] and canine cortical bone [57]), unaffected (canine cortical bone) [22] or increased (human cortical bone) [23] with BP treatment. However, indentation hardness is affected by several different material properties [59]. At first sight, the significantly larger tissue stiffness and trend of higher tissue strength with ALN found in the present study seems to contradict most of the previous studies, reporting no significant change in tissue modulus after alendronate treatment [22,23,27,34,42]. It may well be, however, that the potentially improved material behavior was counterbalanced in these previous studies by other alterations in the tissue, like accumulation of microdamage after BP treatment [8,20]. As tissue strength is usually determined in bending experiments on mm sized cortical bone specimens, it is very likely that microdamage is present in vivo in those samples. In contrast, in the present study individual trabeculae were used for tissue testing (size of 100–300 μm). As individual trabeculae that contain microcracks are very fragile, in comparison to undamaged samples, we assume that only intact, undamaged samples were tested here. Pre-damaged specimens have been very likely destroyed during the dissection, embedding or unmounting procedures. Thus, it is postulated that the tissue/material indeed shows a larger stiffness and strength after BP treatment, but this effect may be counterbalanced at larger scales because of the presence of microdamage.

The non-linear model of Siegmund et al. [21] further predicted a reduced toughness at the level of individual trabeculae after alendronate treatment. Toughness is the material's ability to absorb energy until failure and can be split into elastic work ($\widehat{W}_{el}$) and post-yield work ($\widehat{W}_{py}$). In the present study, neither elastic nor post-yield work were affected by alendronate treatment. This finding is in accordance to literature, where no change of elastic work and only a trend of lower post-yield work was observed at the tissue scale of bending experiments of canine cortical bone [22,42]. Similarly, Tang et al. found no significant change of post-yield work of cortical bone with alendronate or risedronate treatment of beagle dogs at clinical doses, but only at high doses [57]. Decreased bone toughness has also been linked to an accumulation of advanced glycation end-products (AGEs) in human cortical bone [60,61]. As such, also the accumulation of AGEs has been reported to increase in trabecular canine bone with BP treatment [56], but in studies on cortical canine bone, this effect was only significant in high dose regimes [57,62]. The amount of AGEs in the current study is likely only moderately elevated, as clinical doses of alendronate (0.2 mg/kg) were administered. At the whole bone level compression of canine vertebrae indicated an insignificantly lower toughness of BP-treated bone at clinical doses [10,11]. Interestingly, high dose regimes of alendronate treatment of beagle dogs significantly reduced the toughness in compression tests of vertebrae [14], and three-point bending tests on ribs [15,63]. In those studies, a significant accumulation of microdamage has been observed at clinical [11] and high-dose BP-treatment regimens [10,12,14,15]. Interestingly, microdamage was also significantly larger in trabecular bone cores of the femoral head in patients treated for 1–9 years with alendronate [64]. In the present study, we aimed to induce microdamage in individual trabeculae in cyclic tensile tests with increasing amplitudes, as described previously for four-point bending tests on cortical bone prismatic beams [16]. Surprisingly, we did not detect any significant change of stiffness with increasing load cycles (see supplementary Fig. S4), but note that data scatter was large. In accordance to previous studies on bending experiments of cortical beams [65] no significant difference in stiffness loss of BP-treated samples was seen. However, previous studies suggest the fatigue life was significantly reduced after BP-treatment [65,66]. No difference in accumulated damage density was observed in the present study (see Fig. 4), indicating that toughness was unaffected by alendronate treatment perhaps because of a lack of pre-existing microdamage in the trabeculae that were selected for testing. Accordingly, the number of cycles at damage detection also was not affected by alendronate treatment. The tensile modulus determined in each loading cycle (see supplementary material and Fig. S4) was significantly larger for alendronate samples in the first three loading and all unloading cycles, in accordance to the determined increase of apparent elastic modulus and long-term stiffness. Further, the unloading stiffness was significantly larger than the loading stiffness in the first cycle ($p < 0.001$, in all treatment groups). This finding might shed some light on the huge variation of reported values for elastic modulus obtained from different measurement techniques [67]. In nanoindentation elastic modulus is determined in the unloading part, whereas it its determined in the loading part in mechanical tests on individual trabeculae, which might partly explain the observed gap. Further, Turunen et al. confirmed the observed "large strains" (~10%) in tests of individual trabeculae with synchrotron radiation X-ray tomography on compression tests of cancellous bone and related previously smaller reported strains to too small image resolutions [68].

4.2. Raloxifene treatment increases tissue toughness

Tissue toughness of raloxifene-treated samples was higher due to a significantly larger post-yield work ($\widehat{W}_{py}$, $p = 0.002$), compared to control specimens, while elastic work ($\widehat{W}_{el}$) was not affected. The larger post-yield work was mainly related to a significantly larger strain at maximum stress ($\hat{\varepsilon}_{max}$, $p = 0.032$), whereas maximum stress only showed a trend towards larger values in RAL-group samples ($\hat{\sigma}_{max}$, $p = 0.079$). In contrast, yield strain (ε_Y) did not show a significant difference in raloxifene-treated bone samples. These findings are in accordance with literature, where larger tissue toughness has been related to a significantly higher post-yield displacement, while pre-yield displacement was not affected [16]. Interestingly, also ex vivo exposure of canine and human cortical bone beams to raloxifene resulted in a larger post-yield work without affecting elastic work [69]. The authors related the elevated toughness to an increase in matrix bound water. We have also shown in a previous study that removal of free and collagen-bound water of individual trabeculae resulted in an approximately 2-fold decreased post-yield work [36]. Further, Siegmund et al. also predicted an increase of post-yield work, associated with a larger ultimate strain and stress in a non-linear model [21]. Although not significant, maximum stress also tended to be larger in RAL-group samples in the current study (K.W. $p = 0.079$). In contrast, no significant difference of ultimate stress (σ_u), which is determined with the rheological model, was detected between RAL and CON-group samples. Previous studies also did not find a significant difference in ultimate stress [16,69], suggesting that tissue strength is not significantly changed after raloxifene treatment. In the present study neither instantaneous stiffness (E_0), nor long-term stiffness (E_∞) or Maxwell stiffness (E_{mx}) were affected by raloxifene treatment. In the literature, tissue modulus has been reported as being unaffected [69], non-significantly increased [16,70] or predicted to be decreased [21]. Thus, our findings coincidence with previous studies in the assumption that elastic modulus is not relevantly affected by raloxifene treatment.

Induction of microdamage with cyclic tensile testing revealed neither a significant difference in accumulated microdamage nor in change of stiffness in subsequent cycles (see supplementary Fig. S4). In accordance, cyclic four-point bending experiments on cortical bone

specimens indicated no significant difference between raloxifene or saline-treated samples, neither in accumulated microdamage, nor in stiffness loss [16]. However, one may speculate that a larger toughness should also increase the amount of accumulated microdamage, as shown for hydrated trabeculae [36]. On the other hand, damage density was found to be unchanged in vivo after one year treatment with raloxifene in dog vertebrae [11]. In that study by Allen et al., only crack length was significantly longer, which has been assumed to be caused by an increase of length of previously present microcracks. In the current study, no linear microcracks at all could be identified in individual trabeculae. Instead, only diffuse damage was present, which has been determined as the major damage form in tensile regions of four-point bending experiments on cortical bone [71,72] and in tensile tests on individual trabeculae [38]. As already mentioned, individual trabeculae may not have contained pre-existing microcracks, which might explain that damage accumulation was not affected. Although toughness was higher in RAL-group samples, their TMD was not changed. Previously mineralization was also reported to be unaffected by raloxifene treatment [11,69]. Consequently, the improved tissue material properties (toughness) in raloxifene-treated bone are likely to be the main reason for observed superior whole bone strength, independently of bone mineralization (tissue mineralization and bone volume), which is in agreement with Allen et al. [11].

4.3. Limitations

Although micro-mechanical experiments of bone tissue enhance our understanding of changes at the material level, they also have limitations, mainly related to the small size of bone specimens. First, as trabeculae were rather small (~300 μm in length) several samples were damaged during dissection and could not be tested. Thus, there is a potential bias of selected trabeculae, in comparison to the whole population. It can be questioned how representative individual trabeculae are for trabecular bone tissue. However, testing a large number (we aimed for 30 samples and five animals per group) of samples should overcome this limitation. Further, as all samples were treated in the same way it is very unlikely that this bias was different among groups. Nevertheless, it cannot be solely excluded that e.g. more brittle trabeculae were damaged in the alendronate group. But, given that material properties were found to be improved in that group this possibility does not seem very likely. Trabeculae investigated in this study showed a plate-like, rectangular cross-section with an aspect ratio of 1–3, meaning that stress was potentially not homogeneous in the trabecular strut (see inset in Fig. 1A) making it more difficult to capture potential differences between control and alendronate- or raloxifene-treated samples. Further, there is a large biological variation of the geometry and structure of individual trabeculae. Although tensile tests enable a good material characterization, differences in the aspect ratio and length of trabeculae may still show an influence on the derived material properties and explain at least partly the large intra-group deviations. Thus, obtained tissue material and apparent properties may still inherit a structural influence that could also differ among groups. As such, larger trabeculae in the alendronate group might be more mineralized because of their size, as TMD was shown to increase with trabecular thickness [73]. Potentially, the effect of a larger TMD in BP treatment may be attributed to this increase of trabecular thickness. However, the tissue stiffness and strength is still improved at the trabecular scale and highlights a change at the material level after BP treatment. The rheological model is only capable of using engineering stress and strain, but ultimate strain was in the range of 5 to 10%, suggesting that true stress and logarithmic strain would be preferential (avoiding the assumption of small strains). However, deviations between ultimate engineering strain and true strain were small (2.5 to 5%) and still reasonable for ultimate stress (5 to 9%). Microdamage accumulation was used as a stop criterion (whitening) and stained in samples that were tested close to failure. As recognition of whitening and stopping before failure required training and relied on manual action of the operator, some tests could not be stopped before failure. This may have biased the amount of accumulated microdamage. But, evaluation of microdamage of fractured samples indicated no significant difference to samples stopped close to failure, since all samples showed around 30 to 50% damage density in the trabecular strut.

5. Conclusions

The present study evaluated the effect of anti-resorptive treatment on the material properties of individual trabeculae. Evaluation of these properties with our previously developed rheological model highlighted that trabecular bone is not purely linearly elastic, but can be well modeled as an elasto-visco-plastic material. Treatment with alendronate showed a greater apparent tissue elastic modulus, instantaneous as well as long-term stiffness, and maximum stress, compared to healthy bone of controls. In contrast, raloxifene treatment showed a larger toughness and strain at maximum stress. These changes in the material properties can be related to different underlying mechanisms. The larger elastic modulus and maximum stress in alendronate-treated samples is attributed to higher TMD, whereas this was not the case for toughness and the origin of change remains unknown. Taken together, the observed superior whole bone mechanics after anti-resorptive treatment are at least partly related to improved material properties.

Supplementary data to this article can be found online at https://doi.org/10.1016/j.bone.2021.115995.

Funding sources

This work was supported by the Austrian Marshall Plan Foundation. The animal studies were supported by NIH grant 5R01AR047838, and a grant from Lilly Research Labs. Merck and Co. kindly provided the alendronate under a material transfer agreement. The authors further acknowledge TU Wien Bibliothek for financial support through its Open Access Funding Programme.

CRediT authorship contribution statement

Martin Frank: Formal analysis, Data Curation, Writing - Original Draft, Visualization. **Andreas Grabos**: Methodology, Investigation, Funding acquisition. **Andreas G. Reisinger**: Software, Writing - Review and Editing. **David B. Burr**: Animal model development, Data Curation, Writing - Review and Editing. **Dieter H. Pahr**: Supervision, Writing - Review & Editing. **Matthew R. Allen**: Resources, Writing - Review and Editing. **Philipp J. Thurner**: Conceptualization, Supervision, Funding acquisition, Writing - Review & Editing.

Declaration of interest

Dr. Pahr declares involvement in Dr. Pahrs Ingenieurs e.U. All other authors have nothing to disclose.

Acknowledgements

The authors thank Dr. Keith Condon for sharing his expertise in histological staining techniques.

References

[1] L.G. Raisz, G.A. Rodan, Pathogenesis of osteoporosis, Endocrinol. Metab. Clin. N. Am. 32 (2003) 15–24, https://doi.org/10.1016/S0889-8529(02)00055-5.
[2] R. Eastell, C.J. Rosen, D.M. Black, A.M. Cheung, M.H. Murad, D. Shoback, Pharmacological management of osteoporosis in postmenopausal women: an endocrine society clinical practice guideline, J. Clin. Endocrinol. Metab. 104 (2019) 1595–1622, https://doi.org/10.1210/jc.2019-00221.
[3] S. Epstein, The roles of bone mineral density, bone turnover, and other properties in reducing fracture risk during antiresorptive therapy, Mayo Clin. Proc. 80 (2005) 379–388, https://doi.org/10.4065/80.3.379.

[4] H.G. Bone, D. Hosking, J.P. Devogelaer, J.R. Tucci, R.D. Emkey, R.P. Tonino, J. A. Rodriguez-Portales, R.W. Downs, J. Gupta, A.C. Santora, U.A. Liberman, Ten years' experience with alendronate for osteoporosis in postmenopausal women, N. Engl. J. Med. 350 (2004) 1189–1199, https://doi.org/10.1056/NEJMoa030897.

[5] B. Ettinger, B.H. Mitlalc, T. Nickelsen, H.K. Genant, C. Christiansen, J.R. Zanchetta, J. Stakkestad, Reduction of vertebral fracture risk in postmenopausal women with osteoporosis treated with raloxifene, JAMA 282 (1999) 637–645.

[6] P.D. Miller, Bone density and markers of bone turnover in predicting fracture risk and how changes in these measures predict fracture risk reduction, Curr. Osteoporos. Rep. 3 (2005) 103–110, https://doi.org/10.1007/s11914-005-0018-6.

[7] S. Sarkar, B.H. Mitlak, M. Wong, J.L. Stock, D.M. Black, K.D. Harper, Relationships between bone mineral density and incident vertebral fracture risk with raloxifene therapy, J. Bone Miner. Res. 17 (2002) 1–10, https://doi.org/10.1359/jbmr.2002.17.1.1.

[8] M.R. Allen, D.B. Burr, Mineralization, microdamage, and matrix: how bisphosphonates influence material properties of bone, BoneKEy-Osteovision. 4 (2007) 49–60, https://doi.org/10.1138/20060248.

[9] P. Kostenuik, On the Evolution and Contemporary Roles of Bone Remodeling, Fourth Edi, Elsevier, 2013, https://doi.org/10.1016/B978-0-12-415853-5.00037-6.

[10] M.R. Allen, K. Iwata, R. Phipps, D.B. Burr, Alterations in canine vertebral bone turnover, microdamage accumulation, and biomechanical properties following 1-year treatment with clinical treatment doses of risedronate or alendronate, Bone. 39 (2006) 872–879, https://doi.org/10.1016/j.bone.2006.04.028.

[11] M.R. Allen, K. Iwata, M. Sato, D.B. Burr, Raloxifene enhances vertebral mechanical properties independent of bone density, Bone. 39 (2006) 1130–1135, https://doi.org/10.1016/j.bone.2006.05.007.

[12] S. Komatsubara, S. Mori, T. Mashiba, M. Ito, J. Li, Y. Kaji, T. Akiyama, K. Miyamoto, Y. Cao, J. Kawanishi, H. Norimatsu, Long-term treatment of incadronate disodium accumulates microdamage but improves the trabecular bone microarchitecture in dog vertebra, J. Bone Miner. Res. 18 (2003) 512–520, https://doi.org/10.1359/jbmr.2003.18.3.512.

[13] S. Komatsubara, S. Mori, T. Mashiba, J. Li, K. Nonaka, Y. Kaji, T. Akiyama, K. Miyamoto, Y. Cao, J. Kawanishi, H. Norimatsu, Suppressed bone turnover by long-term bisphosphonate treatment accumulates microdamage but maintains intrinsic material properties in cortical bone of dog rib, J. Bone Miner. Res. 19 (2004) 999–1005, https://doi.org/10.1359/JBMR.040126.

[14] T. Mashiba, C.H. Turner, T. Hirano, M.R. Forwood, C.C. Johnston, D.B. Burr, Effects of suppressed bone turnover by bisphosphonates on microdamage accumulation and biomechanical properties in clinically relevant skeletal sites in beagles, Bone. 28 (2001) 524–531, https://doi.org/10.1016/S8756-3282(01)00414-8.

[15] T. Mashiba, T. Hirano, C.H. Turner, M.R. Forwood, C.C. Johnston, D.B. Burr, Suppressed bone turnover by bisphosphonates increases microdamage accumulation and reduces some biomechanical properties in dog rib, J. Bone Miner. Res. 15 (2000) 613–620, https://doi.org/10.1359/jbmr.2000.15.4.613.

[16] M.R. Allen, H.A. Hogan, W.A. Hobbs, A.S. Koivuniemi, M.C. Koivuniemi, D.B. Burr, Raloxifene enhances material-level mechanical properties of femoral cortical and trabecular bone, Endocrinology. 148 (2007) 3908–3913, https://doi.org/10.1210/en.2007-0275.

[17] B. Borah, T.E. Dufresne, P.A. Chmielewski, T.D. Johnson, A. Chines, M.D. Manhart, Risedronate preserves bone architecture in postmenopausal women with osteoporosis as measured by three-dimensional microcomputed tomography, Bone. 34 (2004) 736–746, https://doi.org/10.1016/j.bone.2003.12.013.

[18] M. Ding, J.S. Day, D.B. Burr, T. Mashiba, T. Hirano, H. Weinans, D.R. Sumner, I. Hvid, Canine cancellous bone microarchitecture after one year of high-dose bisphosphonates, Calcif. Tissue Int. 72 (2003) 737–744, https://doi.org/10.1007/s00223-002-2066-6.

[19] R. Recker, P. Masarachia, A. Santora, T. Howard, P. Chavassieux, M. Arlot, G. Rodan, L. Wehren, D. Kimmel, Trabecular bone microarchitecture after alendronate treatment of osteoporotic women, Curr. Med. Res. Opin. 21 (2005) 185–194, https://doi.org/10.1185/030079904X20259.

[20] J.S. Day, M. Ding, P. Bednarz, J.C. van der Linden, T. Mashiba, T. Hirano, C. C. Johnston, D.B. Burr, I. Hvid, D.R. Sumner, H. Weinans, Bisphosphonate treatment affects trabecular bone apparent modulus through micro-architecture rather than matrix properties, J. Orthop. Res. 22 (2004) 465–471, https://doi.org/10.1016/j.orthres.2003.05.001.

[21] T. Siegmund, M.R. Allen, D.B. Burr, Can deterministic mechanical size effects contribute to fracture and microdamage accumulation in trabecular bone? J. Theor. Biol. 265 (2010) 202–210, https://doi.org/10.1016/j.jtbi.2010.04.009.

[22] C. Acevedo, H. Bale, B. Gludovatz, A. Wat, S.Y. Tang, M. Wang, B. Busse, E. A. Zimmermann, E. Schaible, M.R. Allen, D.B. Burr, R.O. Ritchie, Alendronate treatment alters bone tissues at multiple structural levels in healthy canine cortical bone, Bone. 81 (2015) 352–363, https://doi.org/10.1016/j.bone.2015.08.002.

[23] A.A. Lloyd, B. Gludovatz, C. Riedel, E.A. Luengo, R. Saiyed, E. Marty, D.G. Lorich, J.M. Lane, R.O. Ritchie, B. Busse, E. Donnelly, Atypical fracture with long-term bisphosphonate therapy is associated with altered cortical composition and reduced fracture resistance, Proc. Natl. Acad. Sci. U. S. A. 114 (2017) 8722–8727, https://doi.org/10.1073/pnas.1704460114.

[24] D. Pienkowski, C.L. Wood, H.H. Malluche, Young's modulus and hardness of human trabecular bone with bisphosphonate treatment durations up to 20 years, Osteoporos. Int. 30 (2019) 277–285, https://doi.org/10.1007/s00198-018-4760-x.

[25] S. Ma, E.L. Goh, A. Jin, R. Bhattacharya, O.R. Boughton, B. Patel, A. Karunaratne, N.T. Vo, R. Atwood, J.P. Cobb, U. Hansen, R.L. Abel, Long-term effects of bisphosphonate therapy: perforations, microcracks and mechanical properties, Sci. Rep. 7 (2017) 1–10, https://doi.org/10.1038/srep43399.

[26] E.A. Zimmermann, E. Schaible, H. Bale, H.D. Barth, S.Y. Tang, P. Reichert, B. Busse, T. Alliston, J.W. Ager, R.O. Ritchie, Age-related changes in the plasticity and toughness of human cortical bone at multiple length scales, Proc. Natl. Acad. Sci. U. S. A. 108 (2011) 14416–14421, https://doi.org/10.1073/pnas.1107966108.

[27] E.A. Zimmermann, E. Schaible, B. Gludovatz, F.N. Schmidt, C. Riedel, M. Krause, E. Vettorazzi, C. Acevedo, M. Hahn, K. Puschel, S. Tang, M. Amling, R.O. Ritchie, B. Busse, Intrinsic mechanical behavior of femoral cortical bone in young, osteoporotic and bisphosphonate-treated individuals in low-and high energy fracture conditions, Sci. Rep. 6 (2016) 1–12, https://doi.org/10.1038/srep21072.

[28] R.C. Güerri-Fernández, X. Nogués, J.M. Quesada Gõmez, E. Torres Del Pliego, L. Puig, N. García-Giralt, G. Yoskovitz, L. Mellibovsky, P.K. Hansma, A. Díez-Pérez, Microindentation for in vivo measurement of bone tissue material properties in atypical femoral fracture patients and controls, J. Bone Miner. Res. 28 (2013) 162–168, https://doi.org/10.1002/jbmr.1731.

[29] C. Cherraf-Schweyer, G. Maurice, M. Taghite, K. Taous, An experimental and theoretical approach of elasticity and viscoelasticity of compact and spongy bone with periodic homogenization, Comput. Methods Biomech. Biomed. Eng. 10 (2007) 195–207, https://doi.org/10.1080/10255840701284002.

[30] R.S. Lakes, J.L. Katz, Interrelationships among the viscoelastic functions for anisotropic solids: application to calcified tissues and related systems, J. Biomech. 7 (1974) 259–270.

[31] R.S. Lakes, J.L. Katz, S.S. Sternstein, Viscoelastic properties of wet cortical bone-I. Torsional and biaxial studies, J. Biomech. 12 (1979), https://doi.org/10.1016/0021-9290(79)90016-2.

[32] M.R. Allen, D.B. Burr, Bisphosphonate effects on bone turnover, microdamage, and mechanical properties: what we think we know and what we know that we don't know, Bone. 49 (2011) 56–65, https://doi.org/10.1016/j.bone.2010.10.159.

[33] A.H. Warriner, N.M. Patkar, J.R. Curtis, E. Delzell, L. Gary, M. Kilgore, K.G. Saag, Which fractures are most attributable to osteoporosis? Amy J. Clin. Epidemiol. 64 (2016) 46–53, https://doi.org/10.1016/j.physbeh.2017.03.040.

[34] M. Krause, M. Soltau, E.A. Zimmermann, M. Hahn, J. Kornet, A. Hapfelmeier, S. Breer, M. Morlock, B. Wulff, K. Püschel, C.C. Glueer, M. Amling, B. Busse, Effects of long-term alendronate treatment on bone mineralisation, resorption parameters and biomechanics of single human vertebral trabeculae, Eur. Cells Mater. 28 (2014) 152–165, https://doi.org/10.22203/eCM.v028a12.

[35] A.G. Reisinger, M. Frank, P.J. Thurner, D.H. Pahr, A two - layer elasto - visco - plastic rheological model for the material parameter identification of bone tissue, Biomech. Model. Mechanobiol. (2020), https://doi.org/10.1007/s10237-020-01329-0.

[36] M. Frank, D. Marx, V. Nedelkovski, J.T. Fischer, D.H. Pahr, P.J. Thurner, Dehydration of individual bovine trabeculae causes transition from ductile to quasi-brittle failure mode, J. Mech. Behav. Biomed. Mater. 87 (2018) 296–305, https://doi.org/10.1016/j.jmbbm.2018.07.039.

[37] M. Frank, D. Marx, D.H. Pahr, P.J. Thurner, Mechanical properties of individual trabeculae in a physiological environment, Proc. 13th IASTED Int. Conf. Biomed. Eng. BioMed. 2017 (2017) 141–146, https://doi.org/10.2316/P.2017.852-023.

[38] M. Frank, J.-T.T. Fischer, P.J. Thurner, Microdamage formation in individual bovine trabeculae during fatigue testing, J. Biomech. 115 (2021), https://doi.org/10.1016/j.jbiomech.2020.110131.

[39] P.J. Thurner, B. Erickson, R. Jungmann, Z. Schriock, J.C. Weaver, G.E. Fantner, G. Schitter, D.E. Morse, P.K. Hansma, High-speed photography of compressed human trabecular bone correlates whitening to microscopic damage, Eng. Fract. Mech. 74 (2007) 1928–1941, https://doi.org/10.1016/j.engfracmech.2006.05.024.

[40] T.C. Lee, S. Mohsin, D. Taylor, R. Parkesh, T. Gunnlaugsson, F.J.O. Brien, M. Giehl, W. Gowin, Detecting microdamage in bone, J. Anat. 2050 (2003) 161–172.

[41] A.M. Torres, J.B. Matheny, T.M. Keaveny, D. Taylor, C.M. Rimnac, C.J. Hernandez, Material heterogeneity in cancellous bone promotes deformation recovery after mechanical failure, Proc. Natl. Acad. Sci. U. S. A. 113 (2016) 2892–2897, https://doi.org/10.1073/pnas.1520539113.

[42] D.B. Burr, T. Diab, A. Koivunemi, M. Koivunemi, M.R. Allen, Effects of one to three years treatment with alendronate on mechanical properties of the femoral shaft in a canine model: implications for subtrochanteric femoral fracture risk, J. Orthop. Res. 27 (2009) 1288–1292, https://doi.org/10.1002/jor.20895.EFFECTS.

[43] Y. Bala, B. Depalle, D. Farlay, T. Douillard, S. Meille, H. Follet, R. Chapurlat, J. Chevalier, G. Boivin, Bone micromechanical properties are compromised during long-term alendronate therapy independently of mineralization, J. Bone Miner. Res. 27 (2012) 825–834, https://doi.org/10.1002/jbmr.1501.

[44] R. Carretta, B. Luisier, D. Bernoulli, E. Stüssi, R. Müller, S. Lorenzetti, Novel method to analyze post-yield mechanical properties at trabecular bone tissue level, J. Mech. Behav. Biomed. Mater. 20 (2013) 6–18, https://doi.org/10.1016/j.jmbbm.2012.12.003.

[45] J. Currey, Incompatible mechanical properties in compact bone, J. Theor. Biol. 231 (2004) 569–580, https://doi.org/10.1016/j.jtbi.2004.07.013.

[46] J.D. Currey, Tensile yield in compact bone is determined by strain, post-yield behaviour by mineral content, J. Biomech. 37 (2004) 549–556, https://doi.org/10.1016/j.jbiomech.2003.08.008.

[47] P. Garnero, The contribution of collagen crosslinks to bone strength, Bonekey Rep. 1 (2012) 182, https://doi.org/10.1038/bonekey.2012.182.

[48] X. Banse, T.J. Sims, A.J. Bailey, Mechanical properties of adult vertebral cancellous bone: correlation with collagen intermolecular cross-links, J. Bone Miner. Res. 17 (2002) 1621–1628, https://doi.org/10.1359/jbmr.2002.17.9.1621.

[49] X. Wang, X. Shen, X. Li, C.M. Agrawal, Age-related changes in the collagen network and toughness of bone, Bone. 31 (2002) 1–7, https://doi.org/10.1016/S8756-3282(01)00697-4.

[50] X. Wang, R.A. Bank, J.M. TeKoppele, C. Mauli Agrawal, The role of collagen in determining bone mechanical properties, J. Orthop. Res. 19 (2001) 1021–1026, https://doi.org/10.1016/S0736-0266(01)00047-X.
[51] D.B. Burr, The contribution of the organic matrix to bone's material properties, Bone. 31 (2002) 8–11, https://doi.org/10.1016/S8756-3282(02)00815-3.
[52] S. Nobakhti, S.J. Shefelbine, On the relation of bone mineral density and the elastic modulus in healthy and pathologic bone, Curr. Osteoporos. Rep. 16 (2018) 404–410, https://doi.org/10.1007/s11914-018-0449-5.
[53] P. Roschger, S. Rinnerthaler, J. Yates, G.A. Rodan, P. Fratzl, K. Klaushofer, B. Samples, Alendronate increases degree and uniformity of mineralization in cancellous bone and decreases the porosity in cortical bone of osteoporotic women *, Bone. 29 (2001) 185–191.
[54] L. Mulder, J.H. Koolstra, J.M.J. den Toonder, T.M.G.J. van Eijden, Relationship between tissue stiffness and degree of mineralization of developing trabecular bone, J. Biomed. Mater. Res. Part A 84A (2008) 508–515, https://doi.org/10.1002/jbm.a.
[55] N.M.B.K. Willems, L. Mulder, The correlation between mineralization degree and bone tissue stiffness in the porcine mandibular condyle, J. Bone Miner. Metab. 32 (2014) 29–37, https://doi.org/10.1007/s00774-013-0464-7.
[56] M.R. Allen, E. Gineyts, D.B. Burr, Bisphosphonates alter trabecular bone collagen cross-linking and isomerization in beagle dog vertebra, Osteoporos. Int. 19 (2008) 329–337, https://doi.org/10.1007/s00198-007-0533-7.
[57] S.Y. Tang, M.R. Allen, R. Phipps, D.B. Burr, D. Vashishth, Changes in non-enzymatic glycation and its association with altered mechanical properties following 1-year treatment with risedronate or alendronate, Osteoporos. Int. 20 (2009) 887–894, https://doi.org/10.1007/s00198-008-0754-4.
[58] Y. Bala, D. Farlay, R.D. Chapurlat, G. Boivin, Modifications of bone material properties in postmenopausal osteoporotic women long-term treated with alendronate, Eur. J. Endocrinol. 165 (2011) 647–655, https://doi.org/10.1530/EJE-11-0333.
[59] D.P. Fyhrie, B.A. Christiansen, Bone material properties and skeletal fragility bone material properties and skeletal fragility, Calcif. Tissue Int. 97 (2015) 213–228, https://doi.org/10.1007/s00223-015-9997-1.
[60] S.Y. Tang, D. Vashishth, The relative contributions of non-enzymatic glycation and cortical porosity on the fracture toughness of aging bone, J. Biomech. 44 (2011) 330–336, https://doi.org/10.1016/j.jbiomech.2010.10.016.
[61] A.A. Poundarik, P.-C. Wu, Z. Evis, G.E. Sroga, A. Ural, M. Rubin, D. Vashishth, A direct role of collagen glycation in bone fracture, J. Mech. Behav. Biomed. Mater. 52 (2015) 120–130, https://doi.org/10.1016/j.jmbbm.2015.08.012.
[62] M. Saito, S. Mori, S. Komatsubara, Collagen maturity, glycation induced-pentosidine, and mineralization are increased following 3-year treatment with incadronate in dogs, Osteoporos. Int. 19 (2008) 1343–1354, https://doi.org/10.1007/s00198-008-0585-3.
[63] M.R. Allen, S. Reinwald, D.B. Burr, Alendronate reduces bone toughness of ribs without significantly increasing microdamage accumulation in dogs following three years of daily treatment, Calcif. Tissue Int. 82 (2008) 354–360, https://doi.org/10.1038/jid.2014.371.
[64] A. Jin, J. Cobb, U. Hansen, R. Bhattacharya, C. Reinhard, N. Vo, R. Atwood, J. Li, A. Karunaratne, C. Wiles, R. Abel, The effect of long-term bisphosphonate therapy on trabecular bone strength and microcrack density, Bone Jt. Res. 6 (2017) 602–609, https://doi.org/10.1302/2046-3758.610.BJR-2016-0321.R1.
[65] D. Bajaj, J.R. Geissler, M.R. Allen, D.B. Burr, J.C. Fritton, The resistance of cortical bone tissue to failure under cyclic loading is reduced with alendronate, Bone. 64 (2014) 57–64, https://doi.org/10.1016/j.bone.2014.03.045.
[66] G.R. Brock, J.T. Chen, A.R. Ingraffea, J. MacLeay, G.E. Pluhar, A.L. Boskey, M.C. H. van der Meulen, The effect of osteoporosis treatments on fatigue properties of cortical bone tissue, Bone Rep. 2 (2015) 8–13, https://doi.org/10.1016/j.bonr.2014.10.004.
[67] D. Wu, P. Isaksson, S.J. Ferguson, C. Persson, Young's modulus of trabecular bone at the tissue level: a review, Acta Biomater. 78 (2018) 1–12, https://doi.org/10.1016/j.actbio.2018.08.001.
[68] M.J. Turunen, S. Le Cann, E. Tudisco, G. Lovric, A. Patera, S.A. Hall, H. Isaksson, Sub-trabecular strain evolution in human trabecular bone, Sci. Rep. 10 (2020) 1–14, https://doi.org/10.1038/s41598-020-69850-x.
[69] M.A. Gallant, D.M. Brown, M. Hammond, J.M. Wallace, J. Du, J.D. Almer, S. R. Stock, M.R. Allen, B. David, Bone cell-independent benefits of raloxifene on the skeleton: a novel mechanism for improving bone material properties, Bone. 61 (2015) 191–200, https://doi.org/10.1016/j.bone.2014.01.009.
[70] J.C. Burketa, D.J. Brooksa, J.M. MacLeayb, S.P. Bakerc, A.L. Boskey, M.C.H. van der Meulen, Variations in nanomechanical properties and tissue composition within trabeculae from an ovine model of osteoporosis and treatment, Bone. 52 (2013) 326–336, https://doi.org/10.1016/j.bone.2012.10.018.
[71] T. Diab, D. Vashishth, Effects of damage morphology on cortical bone fragility, Bone. 37 (2005) 96–102, https://doi.org/10.1016/j.bone.2005.03.014.
[72] T.M. Boyce, D.P. Fyhrie, M.C. Glotkowski, E.L. Radin, M.B. Schaffler, Damage type and strain mode associations in human compact bone bending fatigue, J. Orthop. Res. 16 (1998) 322–329, https://doi.org/10.1002/jor.1100160308.
[73] L. Mulder, J.H. Koolstra, W.A. Weijs, T.M.G.J. Van Eijden, Architecture and mineralization of developing trabecular bone in the pig mandibular condyle, Anat. Rec. Part A Discov. Mol. Cell. Evol. Biol. 285 (2005) 659–666, https://doi.org/10.1002/ar.a.20208.
[74] M. Doube, M.M. Klosowski, A.M. Wiktorowicz-Conroy, J.R. Hutchinson, S. J. Shefelbine, Trabecular bone scales allometrically in mammals and birds, Proc. Biol. Sci. 278 (1721) (2011) 3067–3073, https://doi.org/10.1098/rspb.2011.0069.